Inorg. Chem. **2006**, *45*, 4413–4422

Influence of the Counterion and the Solvent Molecules in the Spin Crossover System $[Co(4\text{-terpyridone})_2]X_p \cdot nH_2O$

Ana Galet,[‡] Ana Belén Gaspar,[†] M. Carmen Muñoz,[‡] and José Antonio Real*[,†]

Institut de Ciència Molecular, Departament de Química Inorgánica, Universitat de València, Edifici de Instituts de Paterna, Apartat de Correus 22085, 46071 València, Spain, and Departament de Física Aplicada, Universitat Politécnica de València, Camí de Vera s/n, 46022, València, Spain

Received January 17, 2006

A series of new complexes belonging to the $[Co(4\text{-terpyridone})_2]X_p \cdot nS$ family (4-terpyridone = 2,6-bis(2-pyridyl)-4(1*H*)-pyridone) have been synthesized and characterized, using X-ray single crystal determination and magnetic susceptibility studies, to be X = $[BF_4]^-$ ($p = 2$) and S = H_2O for polymorphs **1** and **2**, X = $[BF_4]^-$ ($p = 1$) and $[SiF_6]^{2-}$ ($p = 0.5$) and S = CH_3OH for **3**, X = $[SiF_6]^{2-}$ ($p = 1$) and S = $3CH_3OH$ and H_2O for **4**, X = $[Co(NCS)_4]^{2-}$ ($p = 1$) and S = $0.5CH_3OH$ for **5**, X = I^- ($p = 2$) and S = $5H_2O$ for **6**, X = $[PF_6]^-$ ($p = 1$) for **7**, and X = $[NO_3]^-$ ($p = 2$) for **8**. Compounds **1**–**7** can be grouped in three sets according to the space group in which they crystallize: (i) $P\bar{1}$ triclinic (**1**, **3**), (ii) $P2_1$ monoclinic (**2**), and (iii) $P2_1/c$ monoclinic (**4**–**7**). The tridentate 4-terpyridone ligands coordinate the Co(II) ions in a mer fashion defining essentially tetragonally compressed $[CoN_6]$ octahedrons. The Co–N axial bonds involving the pyridone rings are markedly shorter than the Co–N equatorial bonds collectively denoted as $Co–N_{central}$ and $Co–N_{distal}$, respectively. The differences in the average $Co–N_{central}$ or $Co–N_{distal}$ distances observed for **1**–**7** reflect the different spin states of Co(II). Complexes **7** and **4′** are fully high spin (HS), while **5** and **6** are low spin (LS). However, the counterion $[Co(NCS)_4]^{2-}$ in complex **5** is high spin. Complexes **1**, **2**, **3**, and **8** exhibit spin-crossover behavior in the 400–100 K temperature region. Compounds **1** and **2** are polymorphs, and interestingly, **1** irreversibly transforms into **2** above 340 K because of a crystallographic phase transition which involves a drastic modification of the crystal packing. The relevant thermodynamic parameters associated with the spin transition of polymorph **2** have been estimated using the regular solution theory leading to $\Delta H = 3.04$ kJ mol^{-1}, $\Delta S = 20$ J K^{-1} mol^{-1}, and $\Gamma = 0.95$ kJ mol^{-1}.

Introduction

Spin-crossover (SCO) materials display labile electronic configurations switchable between the high-spin and low-spin states leading to distinctive changes in magnetism, color, and structure, which may be driven by a variation of temperature or pressure and by light irradiation.[1] Their magnetic, optical, and structural properties may be altered drastically in a narrow range of temperature or pressure for cooperative spin transitions. Cooperativity may be accompanied by hysteresis (memory effect) when the cohesive forces, communicating between the SCO centers in the solid state, propagate the structural changes cooperatively to the whole lattice.[2−4] This confers a bistable character to the material. The so-called SCO phenomenon is observed in six-coordinate transition-metal ions with $3d^n$ ($n = 4-7$) electronic configurations. A crossover between the HS and LS configurations occurs when the $\Delta G_{HL} = G_{HS} - G_{LS}$ is in the range of the thermal energy.

The vast majority of SCO compounds reported so far concerns Fe(II) and Fe(III) complexes, to a lesser extent Co(II),[5] and only in a few cases Mn(III) and Cr(II) complexes.[6] This fact has been explained on the grounds of ligand field

* To whom correspondence should be addressed. E-mail: jose.a.real@uv.es.
† Universitat de València.
‡ Universitat Politécnica de València.

(1) *Spin Crossover in Transition Metal Compounds III*; Gütlich, P., Goodwin, H. A., Eds; Topics in Current Chemistry 233−235; Springer: Berlin, 2004.
(2) Gütlich, P.; Hauser, A.; Spiering, H. *Angew. Chem., Int. Ed. Engl.* **1994**, *33*, 2024.
(3) Real, J. A.; Gaspar, A. B.; Niel, V.; Muñoz, M. C. *Coord. Chem. Rev.* **2003**, *236*, 121.
(4) Real, J. A.; Gaspar, A. B.; Muñoz, M. C. *Dalton Trans.* **2005**, 2062.
(5) Goodwin, H. A. *Top. Curr. Chem.* **2004**, *234*, 49.
(6) Gütlich, P.; Garcia, Y. *Top. Curr. Chem.* **2004**, *234*, 23.

10.1021/ic060090u CCC: $33.50 © 2006 American Chemical Society
Published on Web 05/05/2006

theory.[6] Compared to Fe(II) and Fe(III) ions, which involve the transfer of two electrons during the SCO, the Co(II) experiences a change between the $^2E(t_{2g}^6eg^1)$ and $^4T_1(t_{2g}^5eg^2)$ ground states involving the transfer of just one electron. This is the cause of the important structural, thermodynamic, and kinetic differences observed in the Co(II) SCO behavior with respect Fe(II) and Fe(III) complexes.[5] A change of approximately 0.10, 0.15, and 0.20 Å in metal−donor atom distances takes place concomitantly with the spin conversion in Co(II), Fe(III), and Fe(II) complexes, respectively. The molecular volume changes associated with the spin transition in Co(II) is less pronounced than that in Fe(II) and Fe(III), which explain, in the vast majority of instances, the continuous character of the spin transition in Co(II) complexes. Probably, this is one of the main reasons why Co(II) spin-crossover complexes have been scarcely explored. Despite this fact, discrete mono-,[7−16] di-,[17,18] and trinuclear,[19−21] species, as well as 1D[22] polymeric Co(II) spin-crossover complexes have been reported so far. The most extensively studied are $[Co(terpy)_2]X_2 \cdot nH_2O$ (terpy = 2,2′:6′,2″-terpyridine; X = halide, pseudohalide, NO_3^-, ClO_4^-; $n = 0.5$, 1),[7,8] and $[Co(H_2\text{-fsa}_2\text{en})L_2]$ (H_2-fsa$_2$en = *N*,*N*′-*o*-ethylene-bis-(3-carboxysalicylaldiiminate); L = pyridine, substituted pyridines, and H_2O).[9−12] This second series of compounds exhibits the most abrupt transitions ever observed for Co(II) complexes.

The influence of the anion on the SCO behavior was first observed for salts of $[Co(terpy)_2]^{2+}$. Displacement of the transition temperature, modification of the cooperative behavior (abrupt versus continuous transitions), even stabilization of the HS configuration can be the result of this influence. Recently, we reported preliminary results on the new Co(II) spin-crossover family $[Co(4\text{-terpyridone})_2]X_p \cdot nH_2O$, where 4-terpyridone is the terpy-like ligand 2,6-bis-(2-pyridyl)-4(1*H*)-pyridone and X = SO_4^{2-}, ClO_4^-, and Cl^-, in which the SCO behavior strongly depends on the nature of anion.[23] The SCO and its characteristics (T_c, hysteresis) are governed by subtle structural and electronic modifications tuned by the crystal packing, which determines the ligand-field strength and the SCO behavior. These modifications depend essentially on the nature of the ligands, the noncoordinating anions, the solvent molecules, and the crystal packing. Complete control of these variables is a rather difficult task to accomplish. In addition, their effects are not always consistent from one system to another and in general are not predictable.[4] Indeed, a more systematic investigation of such subfactors is required. In this regard, we report here the synthesis, structure, and magnetic properties of new members of the $[Co(4\text{-terpyridone})_2]X_p \cdot nS$ family where X = $[BF_4]^-$ ($p = 2$) and S = H_2O for polymorphs **1** and **2**, X = $[BF_4]^-$ ($p = 1$) and $[SiF_6]^{2-}$ ($p = 0.5$) and S = CH_3OH for **3**, X = $[SiF_6]^{2-}$ ($p = 1$) and S = $3CH_3OH$ and H_2O for **4**, X = $[Co(NCS)_4]^{2-}$ ($p = 1$) and S = $0.5CH_3OH$ for **5**, X = I^- ($p = 2$) and S = $5H_2O$ for **6**, X = $[PF_6]^-$ ($p = 1$) for **7**, and X = $[NO_3]^-$ ($p = 2$) for **8**.

Experimental Section

Materials. $Co(BF_4)_2 \cdot 6H_2O$, $Co(NO_3)_2 \cdot 6H_2O$, $Co(NCS)_2$, CoI_2, $(NH_4)_2SiF_6$, $AgPF_6$, and 2,6-bis(2-pyridyl)-4(1*H*)-pyridone were purchased from commercial sources and used as received.

Synthesis of 1−8. The synthesis of compounds **1**−**8** has been performed under an argon atmosphere. The preparation of the methanolic solutions containing Co(II) and the appropriate anion depends on X. $Co(X)_2 \cdot nH_2O$ (1 mmol, 15 mL) was used when X = BF_4^- ($n = 6$) (compounds **1**, **2**), $[Co(NCS)_4]^{2-}$ ($n = 0$) (**5**), I^- ($n = 0$) (**6**), and NO_3^- ($n = 6$) (**8**), while methanolic solutions (15 mL) containing Co(II)/SiF_6^{2-} (**4**) or Co(II)/PF_6^- (**7**) were prepared by dissolving together $CoCl_2 \cdot 6H_2O$ (1 mmol) and an excess of $(NH_4)_2SiF_6$ (4 mmol) or by metathesis from $CoCl_2 \cdot 6H_2O$ (1 mmol) and $AgPF_6$ (2 mmol), respectively. The resulting Co(II)/X were added to a methanolic solution of 4-terpyridone (2 mmol, 15 mL) under continuous stirring. The resulting orange-brown solutions were allowed to evaporate (5−7 days) to produce prismatic brown crystals of **1**−**4**, **7**, and **8** and green crystals of **5**. The crystals were separated by filtration and dried in an argon stream.

It deserves to be noted that **1** and **2** are two polymorphs that form after partial evaporation of the $Co(BF_4)_2 \cdot 6H_2O$/4-terpyridone solutions depending on their water content. Polymorph **1** forms when the synthesis is carried out in pure methanol, while preferential crystallization of polymorph **2** takes place when the $Co(BF_4)_2 \cdot 6H_2O$ solution is prepared in water instead of methanol. Both polymorphs can be differentiated by their magnetic behavior and powder and single-crystal X-ray diffraction patterns. Another important fact is the rapid hydrolysis of the $[BF_4]^-$ group observed in the $Co(BF_4)_2 \cdot 6H_2O$/4-terpyridone 1:1 methanol/water solutions, which allows the formation of $[SiF_6]^{2-}$ when a standard borosilicate-based reaction vessel is used. Under these conditions, single crystals of $\{[Co(4\text{-terpyridone})](BF_4)(SiF_6)_{0.5} \cdot CH_3OH\}$ (compound **3**) were formed. This compound has also been synthesized directly by mixing stoichiometric amounts of $Co(BF_4)_2 \cdot 6H_2O$ and $(NH_4)_2SiF_6$ and 4-terpyridone in methanol. Surprisingly, in the case of compound **7**, there is only one $[PF_6]^-$ ion per molecule of complex indicating that one keto-enol OH group is deprotonated spontaneously. Yield: 65% (**1**); 40% (**2**); 45% (**3**); 65% (**4**); 80% (**5**); 30% (**6**); 60% (**7**); 25% (**8**). Anal. Calcd for $C_{30}H_{24}B_2F_8O_3N_6Co$ (**1**): C,

(7) Kremer, S.; Henke, W.; Reinen, D. *Inorg. Chem.* **1982**, *21*, 3013.
(8) Figgis, B. N.; Kucharski, E. S.; White, A. W. *Aust. J. Chem.* **1983**, *36*, 1527.
(9) Kahn, O.; Claude, R.; Coudane, H. *Nouv. J. Chim.* **1980**, *4*, 167.
(10) (a) Zarembowitch, J.; Claude, R.; Kahn, O. *Inorg. Chem.* **1985**, *24*, 1576. (b) Zarembowitch, J. *New J. Chem.* **1992**, *16*, 255.
(11) Zarembowitch, J.; Kahn, O. *Inorg. Chem.* **1984**, *23*, 589.
(12) Thuéry, P.; Zarembowitch, J. *Inorg. Chem.* **1986**, *25*, 2001.
(13) Faus, J.; Julve, M.; Lloret, F.; Real, J. A.; Seletten, J. *Inorg. Chem.* **1994**, *33*, 5535.
(14) Mizuno, K.; Lunsford, J. H. *Inorg. Chem.* **1983**, *22*, 3484.
(15) Tiwary, S. K.; Vasudevan, S. *Inorg. Chem.* **1998**, *37*, 5239.
(16) Sieber, R.; Decurtins, S.; Stoeckli-Evans, H.; Wilson, C.; Yifit, D.; Howard, J. A. K.; Capelli, S. C.; Hauser, A. *Chem.—Eur. J.* **2000**, *6*, 361.
(17) Brooker, S.; Plieger, P. G.; Moubaraki, B.; Murray, K. S. *Angew. Chem., Int. Ed.* **1999**, *38*, 408.
(18) Brooker, S.; De Geest, D. J.; Kelly, R. J.; Plieger, P. G.; Moubaraki, B.; Murray, K. S.; Jameson, G. B. *J. Chem. Soc., Dalton Trans.* **2002**, 2080.
(19) Clérac, R.; Cotton, F. A.; Daniels, L. M.; Dunbar, K. R.; Kirschbaum K.; Murillo, C. A.; Pinkerton, A. A.; Schultz, A. J.; Wang, X. *J. Am. Chem. Soc.* **2000**, *122*, 6226.
(20) Clérac, R.; Cotton, F. A.; Dunbar, K. R.; Murillo, C. A.; Wang, X. *Inorg. Chem.* **2001**, *40*, 1256.
(21) Clérac, R.; Cotton, F. A.; Dunbar, K. R.; Lu, T.; Murillo, C. A.; Wang, X. *J. Am. Chem. Soc.* **2000**, *122*, 2272.
(22) Hayami, S.; Hashiguchi, K.; Juhász, G.; Ohba, M.; Ohkawa, H.; Maeda, Y.; Kato, K.; Osaka, K.; Takata, M.; Inoue, K. *Inorg. Chem.* **2004**, *43*, 4124.
(23) Gaspar, A. B.; Muñoz, M. C.; Real, J. A. *Inorg. Chem.* **2001**, *40*, 9.

Table 1. Crystal Data for **1**, **2**, and **3**

	1	**2**	**3** (293 K)	**3** (105 K)
empirical formula	$C_{30}H_{24}N_6O_3B_2F_8Co$	$C_{30}H_{24}N_6O_3B_2F_8Co$	$C_{31}H_{26}N_6O_3B_1F_7Si_{0.5}Co$	
M_r	749.10	749.10	747.36	
cryst syst	triclinic	monoclinic	triclinic	
space group	$P\bar{1}$	$P2_1$	$P\bar{1}$	
a (Å)	8.6953(6)	8.8090(3)	8.6560(2)	8.5470(2)
b (Å)	9.3235(10)	9.0510(4)	9.0430(2)	8.9570(2)
c (Å)	20.240(2)	20.0860(9)	19.8460(7)	19.7260(4)
α (deg)	78.63(9)		84.5610(10)	84.2990(19)
β (deg)	78.282(7)	99.0060(16)	87.5670(10)	86.8180(10)
γ (deg)	87.780(7)		86.2920(10)	86.7140(10)
V (Å^3)	1575.2(3)	1581.72(11)	1542.21(7)	1498.31(6)
Z	2	2	2	
D_c (mg cm^{-3})	1.579	1.573	1.609	1.657
F(000)	758	758	760	
μ(Mo Kα) (mm^{--1})	0.636	0.634	0.664	0.683
cryst size (mm)	0.04 × 0.06 × 0.08	0.05 × 0.05 × 0.10	0.03 × 0.04 × 0.06	
temp (K)	293(2)	293(2)	293(2)	105(2)
total reflns	5504	6107	6963	6691
reflns [$I > 2\sigma(I)$]	2550	4865	4309	5651
R1[a] [$I > 2\sigma(I)$]	0.0950	0.0659	0.0530	0.0498
wR2[a] [$I > 2\sigma(I)$]	0.2185	0.1843	0.1252	0.1561
S	1.010	0.872	1.002	1.005

[a] $R1 = \sum||F_o| - |F_c||/\sum|F_o|$; $wR2 = [\sum[w(F_o^2 - F_c^2)^2]/\sum[w(F_o^2)^2]]^{1/2}$; $w = 1/[\sigma^2(F_o^2) + (mP)^2 + nP]$, where $P = (F_o^2 + 2F_c^2)/3$; $m = 0.1400$ (**1**), 0.1812 (**2**), 0.0776 (**3** HS), and 0.1402 (**3** LS); $n = 0.0000$ (**1**), 0.0000 (**2**), 0.0000 (**3** HS), and 3.0028 (**3** LS).

48.06; H, 3.20; N, 11.21. Found: C, 48.01; H, 3.15; N, 11.18. Anal. Calcd for $C_{30}H_{24}B_2F_8O_3N_6Co$ (**2**): C, 48.06; H, 3.20; N, 11.21. Found: C, 48.07; H, 3.18; N, 11.20. Anal. Calcd for $C_{31}H_{26}BF_7O_3N_6CoSi_{0.5}$ (**3**): C, 49.78; H, 3.48; N, 11.24. Found: C, 49.41; H, 3.45; N, 11.21. Anal. Calcd for $C_{33}H_{36}F_6O_6N_6SiCo$ (**4**): C, 48.68; H, 4.43; N, 10.33. Found: C, 48.41; H, 4.42; N, 10.21. Anal. Calcd for $C_{34.5}H_{24}S_4O_{2.5}N_{10}Co_2$ (**5**): C, 47.89; H, 2.77; N, 16.19. Found: C, 48.01; H, 3.00; N, 16.18. Anal. Calcd for $C_{30}H_{32}I_2O_7N_6Co$ (**6**): C, 39.94; H, 3.55; N, 9.32. Found: C, 40.01; H, 3.35; N, 9.18. Anal. Calcd for $C_{30}H_{21}F_6O_2N_6PCo$ (**7**): C, 51.32; H, 2.99; N, 11.97. Found: C, 51.21; H, 2.75; N, 12.03. Anal. Calcd for $C_{30}H_{22}O_8N_8Co$ (**8**): C, 52.82; H, 3.22; N, 16.43. Found: C, 52.78; H, 3.20; N, 16.41.

X-ray Crystallographic Study. Diffraction data for all complexes was collected with a Nonius Kappa-CCD single-crystal diffractometer using Mo Kα radiation ($\lambda = 0.71073$ Å). A multiscan absorption correction was found to have no significant effect on the refinement results. The structures were solved by direct methods using SHELXS-97 and refined by full-matrix least-squares on F^2 using SHELXL-97.[24] All non-hydrogen atoms were refined anisotropically.

Magnetic Susceptibility Measurements. The variable-temperature magnetic susceptibility measurements were performed on small single crystals using a Quantum Design MPMS2 SQUID susceptometer equipped with a 5.5 T magnet, operating at 1 T and 1.8−400 K. Experimental data were corrected for diamagnetism using Pascal's constants.

Results

Crystal Structures. Compounds **1**−**7** can be grouped in three sets according to the space group in which they crystallize: (i) $P\bar{1}$ triclinic (**1**, **3**), (ii) $P2_1$ monoclinic (**2**), and (iii) $P2_1/c$ monoclinic (**4**−**7**). Tables 1−5 present the relevant crystallographic data, as well as a selection of bond distances and angles and short intermolecular contacts. It is worthwhile mentioning that compound **2** is isotructural with the already reported perchlorate derivative.[23]

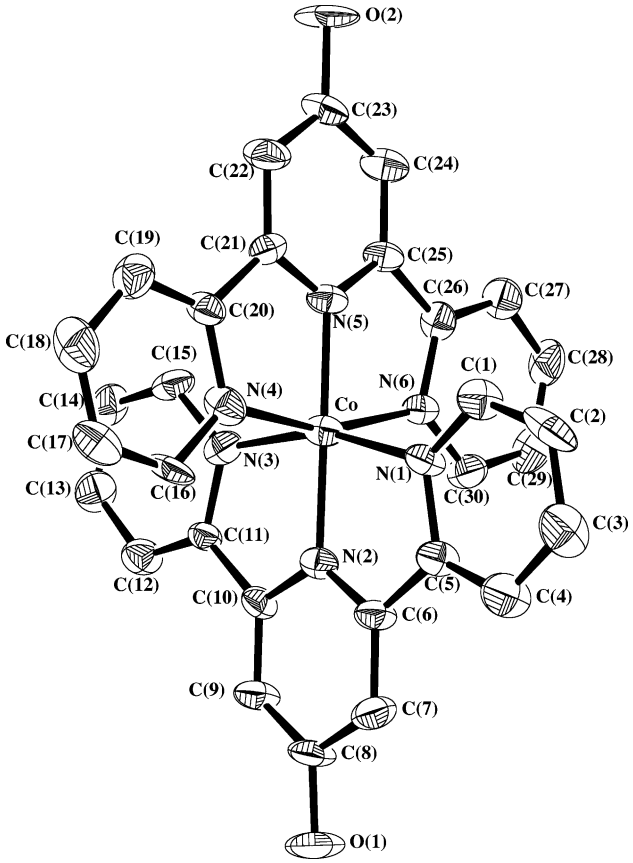

Figure 1. Molecular structure of the cation [Co(4-terpyridone)$_2$]$^{2+}$ with the corresponding non-hydrogen atom numbering. Thermal vibrational ellipsoids are at the 50% probability level, and hydrogen atoms are omitted for clarity.

Molecular Structure of the Cation. Compounds **1**−**6** are made up of discrete cationic complexes [Co(4-terpyridone)$_2$]$^{2+}$, anions, and solvent molecules. As indicated in the

(24) G. M. Sheldrick, *SHELX97, Program for Crystal Structure Determination*; University of Göttingen: Göttingen, Germany, 1997.

Table 2. Crystal Data for **4**−**7**

	4	**5**	**6**	**7**
formula	$C_{33}H_{36}N_6O_6Si_1F_6Co$	$C_{34.5}H_{24}N_{10}O_{2.5}S_4Co_2$	$C_{30}H_{32}N_6O_7I_2Co$	$C_{30}H_{21}N_6O_2PF_6Co$
M_r	811.68	864.74	899.33	701.44
cryst syst	monoclinic	monoclinic	monoclinic	monoclinic
space group	$P2_1/c$	$P2_1/c$	$P2_1/c$	$P2_1/c$
a (Å)	8.7770(2)	11.9290(3)	8.8850(2)	9.3490(2)
b (Å)	22.1790(4)	19.2730(5)	21.9600(5)	21.9440(5)
c (Å)	18.4970(4)	18.4020(6)	18.7530(5)	15.6410(3)
β (deg)	91.8480(10)	114.7970(10)	113.3340(10)	114.2070(10)
V (Å^3)	3598.85(13)	3840.68(19)	3359.72(14)	2926.67(11)
Z	4	4	4	4
D_c (mg cm^{-3})	1.502	1.495	1.782	1.592
F(000)	1676	1756	1772	1420
μ(Mo Kα) (mm^{-1})	0.594	1.129	1.403	0.720
cryst size (mm)	0.03 × 0.05 × 0.07	0.05 × 0.07 × 0.09	0.06 × 0.05 × 0.03	0.05 × 0.05 × 0.02
temp (K)	293(2)	293(2)	293(2)	293(2)
total reflns	8071	8602	4961	6590
reflns [$I > 2\sigma(I)$]	4720	5309	3283	3827
R_1[a] [$I > 2\sigma(I)$]	0.0845	0.0691	0.0478	0.0488
wR2[a]	0.2163	0.1830	0.1250	0.1139
S	0.975	1.013	0.878	0.891

[a] $R1 = \sum||F_o| - |F_c||/\sum|F_o|$; $wR2 = [\sum[w(F_o^2 - F_c^2)^2]/\sum[w(F_o^2)^2]]^{1/2}$; $w = 1/[\sigma^2(F_o^2) + (mP)^2 + nP]$, where $P = (F_o^2 + 2F_c^2)/3$; $m = 0.1340$ (**4**), 0.1087 (**5**), 0.1058 (**6**), and 0.0899 (**7**); $n = 9.4006$ (**4**), 5.8346 (**5**), 6.7702 (**6**), and 0.0000 (**7**).

Table 3. Selected Bond Lengths (Å) and Angles (deg) for **1**, **2**, and **3**

	1	**2**	**3** (293 K)	**3** (105 K)
Co−N(1)	2.027(7)	2.158(5)	2.010(2)	1.974(3)
Co−N(2)	1.909(6)	1.952(4)	1.894(2)	1.871(3)
Co−N(3)	2.036(7)	2.148(5)	2.030(2)	1.986(3)
Co−N(4)	2.007(7)	2.087(4)	2.162(2)	2.183(3)
Co−N(5)	1.892(6)	1.949(4)	1.946(2)	1.943(3)
Co−N(6)	2.021(7)	2.091(4)	2.171(2)	2.183(3)
N(1)−Co−N(2)	80.5(3)	77.8(2)	80.69(10)	81.67(11)
N(1)−Co−N(3)	161.0(3)	155.73(17)	160.69(10)	162.69(12)
N(1)−Co−N(4)	91.9(3)	90.63(17)	92.11(9)	91.86(11)
N(1)−Co-N(5)	101.0(3)	102.6(2)	102.22(10)	100.92(11)
N(1)−Co−N(6)	90.5(3)	93.11(17)	89.83(9)	89.30(10)
N(2)−Co−N(3)	80.6(3)	78.0(2)	80.03(10)	81.04(11)
N(2)−Co−N(4)	99.5(3)	102.63(17)	104.92(10)	104.66(11)
N(2)−Co−N(5)	178.3(3)	178.7(2)	175.74(10)	176.23(11)
N(2)−Co−N(6)	99.7(3)	100.90(16)	98.95(10)	99.01(11)
N(3)−Co−N(4)	89.5(3)	92.83(17)	91.74(9)	91.72(11)
N(3)−Co−N(5)	98.0(3)	101.6(2)	97.09(10)	96.39(11)
N(3)−Co−N(6)	94.3(3)	93.24(18)	94.27(9)	94.19(11)
N(4)−Co−N(5)	81.2(3)	78.66(18)	78.21(10)	78.09(11)
N(4)−Co−N(6)	160.8(3)	156.44(18)	156.05(10)	156.22(11)
N(5)−Co−N(6)	79.6(3)	77.82(18)	78.05(10)	78.37(11)

Table 4. Selected Bond Lengths (Å) and Angles (deg) for **4**−**7**

	4	**5**	**6**	**7**
Co(1)−N(1)	2.083(5)	1.950(4)	1.947(6)	2.157(3)
Co(1)−N(2)	1.904(4)	1.856(4)	1.869(6)	2.018(2)
Co(1)−N(3)	2.089(5)	1.955(4)	1.945(6)	2.157(3)
Co(1)−N(4)	2.093(5)	1.944(4)	1.946(6)	2.158(3)
Co(1)−N(5)	1.906(4)	1.862(4)	1.849(6)	2.039(2)
Co(1)−N(6)	2.096(4)	1.948(4)	1.956(6)	2.180(3)
Co(2)−N(7)		1.945(6)		
Co(2)−N(8)		1.953(5)		
Co(2)−N(9)		1.946(5)		
Co(2)−N(10)		1.950(6)		
N(1)−Co(1)−N(2)	79.07(18)	82.40(16)	82.2(3)	76.59(10)
N(1)−Co(1)−N(3)	158.10(18)	164.86(16)	164.0(2)	152.65(10)
N(1)−Co(1)−N(4)	94.18(17)	91.25(17)	91.7(2)	93.62(10)
N(1)−Co(1)−N(5)	103.04(18)	97.92(17)	97.1(3)	102.96(10)
N(1)−Co(1)−N(6)	88.10(17)	90.27(16)	92.0(2)	91.34(10)
N(2)−Co(1)−N(3)	79.32(18)	82.46(17)	81.9(3)	76.46(10)
N(2)−Co(1)−N(4)	97.66(18)	97.13(17)	97.1(2)	111.08(10)
N(2)−Co(1)−N(5)	176.51(18)	179.54(17)	179.2(3)	173.18(10)
N(2)−Co(1)−N(6)	103.25(18)	98.30(17)	98.6(2)	97.14(10)
N(3)−Co(1)−N(4)	92.15(17)	91.05(18)	91.3(2)	91.70(10)
N(3)−Co(1)−N(5)	98.71(18)	97.22(17)	98.8(3)	104.35(10)
N(3)−Co(1)−N(6)	93.43(18)	91.48(17)	89.3(2)	96.55(9)
N(4)−Co(1)−N(5)	79.47(18)	82.54(16)	82.6(2)	75.72(10)
N(4)−Co(1)−N(6)	159.01(19)	164.55(16)	164.3(2)	151.74(10)
N(5)−Co(1)−N(6)	79.68(17)	82.03(16)	81.8(3)	76.05(10)
N(7)−Co(2)−N(8)		103.0(3)		
N(7)−Co(2)−N(9)		114.3(3)		
N(7)−Co(2)−N(10)		106.9(3)		
N(8)−Co(2)−N(9)		116.2(2)		
N(8)−Co(2)−N(10)		109.4(3)		
N(9)−Co(2)−N(10)		106.7(2)		

Experimental Section one of the keto-enol OH groups is deprotonated in the case of **7** leading to a monocationic [Co(4-terpyridone)(4-terpyridonate)]$^+$ complex. Figure 1 displays the molecular structure of the [Co(4-terpyridone)$_2$]$^{2+}$ complex, together with the corresponding atomic numbering scheme. The tridentate 4-terpyridone ligands coordinate the Co(II) ion in a *mer* fashion defining essentially a tetragonally compressed [CoN$_6$] octahedron. The Co−N(2) and Co−N(5) axial bonds involving the pyridone rings are markedly shorter than the equatorial bonds [Co−N(1), Co−N(3), Co−N(4), and Co−N(6)], collectively denoted here as Co−N$_{central}$ and Co−N$_{distal}$, respectively. The average Co−N$_{central}$ distances are 1.900 (**1**), 1.950 (**2**), 1.920 (293 K) (1.907 Å (105 K)) (**3**), 1.905 (**4**), 1.859 (**5**, **6**), and 2.028 Å (**7**), while the average Co−N$_{distal}$ distances are 2.023 (**1**), 2.121 (**2**), 2.093 (293 K) (2.082 Å (105 K)) (**3**), 2.090 (**4**), 1.949 (**5**, **6**), and 2.163 Å (**7**). The differences in the average Co−N$_{central}$ or Co−N$_{distal}$ distances observed for **1**−**7** reflect the different spin states of Co(II) (vide infra). For instance, the Co(II) ion is fully HS and LS in **7** and **5** or **6**, respectively, but a thermal averaged mixture of both states occurs in **1**, **2**, and **3** (293 K). The N(2)−Co−N(5) angle, which involves the two Co−N$_{central}$ bonds, is very close to the expected for a regular octahedron and is in the 175−179° range. However, the remaining [CoN$_6$] angles reflect the steric constrains imposed by the rigidity of the ligand (i.e., the angles N(1)−Co−N(3) and N(4)−Co−N(6) are in the 152−165° range). It also deserves to be noted that the C(23)−O(2) and C(8)−O(1) distances span from 1.262 to 1.348 Å, indicating that

Table 5. Intermolecular Contacts Shorter than the Sum of the C···C van der Waals (Å) Radii

compound **1**		compound **2**
intralayer	interlayer	intralayer
C(14)···C(2) = 3.472(16)	C(7)···C(7)[a] = 3.533(15)	C(2)···C(14) = 3.553(10)
C(18)···C(30) = 3.451(14)	C(8)···C(7) = 3.480(14)	C(2)···C(15) = 3.511(9)
C(28)···C(19) = 3.519(14)		C(30)···C(17) = 3.548(11)
		C(30)···C(18) = 3.567(10)

compound **3**	compound **4**	compound **5**
intralayer	intralayer	intralayer
C(2)···C(15) = 3.541(4)	C(2)···C(13) = 3.414(10)	C(7)···C(24) = 3.482(6)
C(3)···C(14) = 3.566(4)	C(17)···C(26) = 3.588(8)	C(8)···C(8[b]) = 3.318(9)
C(3)···C(15) = 3.357(4)	C(26)···C(18) = 3.604(8)	C(8)···C(9) = 3.409(9)
C(3)···C(26) = 3.522(4)	C(28)···C(16) = 3.582(9)	
C(4)···C(13) = 3.461(4)	C(29)···C(16) = 3.564(9)	**[Co(NCS)$_4$]$^{2-}$ aromatic rings**
C(5)···C(13) = 3.578(4)		C(31)[c]···C(1) = 3.426(9)
C(5)···C(14) = 3.549(4)		C(31)[c]···C(2) = 3.315(9)
C(15)···C(28) = 3.577(5)		C(32)[c]···C(13) = 3.483(11)
		C(33)[c]···C(18) = 3.479(10)
		C(33)[c]···C(28) = 3.564(10)
		C(33)[c]···C(23) = 3.374(9)

compound **6**	compound **7**	
intralayer	intralayer	interlayer
C(27)···C(18) = 3.529(12)	C(1)···C(2) = 3.480(7)	C(18)···C(30) = 3.558(5)
	C(1)···C(3) = 3.571(7)	
	C(2)···C(2[d]) = 3.424(7)	

[a] Symmetry transformation: $1-x, -y, 1-z$. [b] Symmetry transformation: $-x, -y, 2-z$. [c] The atoms C(31), C(32), and C(33) belongs to the [Co(NCS)$_4$]$^{2-}$ group. [d] Symmetry transformation: $-x, -y, -z$.

the terpyridone ring is present in the enolic form upon coordination.

Crystal Packing. Independently of the space group and cell dimensions, the crystal packing of this series of complex salts can be grouped in two sets. One set involves compounds **1**−**4** and **6**, while the other set concerns **5** and **7**. Figure 2 displays a representative perspective view of the former type. This is a view of the crystal packing along *a* the axis where the molecules lying in the *bc* plane superimpose perfectly (the axes are rotated by 90° around the *a* axis for **4**). The cationic complexes are orientated in this series in a similar way: the line connecting the two opposite OH groups of the 4-terpyridone ligands of the same complex is approximately parallel to the *c* direction (*b* direction in **4**). The lattice can be described as being formed by layers of cationic molecules lying in the *ab* plane (*ac* plane in **4**). The layers stack along the *c* direction (*b* direction in **4**) in such a way that the OH groups of adjacent layers interdigitate. In general, the Co···Co distances within a layer are shorter than those between consecutive layers. The Co···Co distances along the *a* and *b* axes are 8.695(2) and 9.324(2) Å in **1**, 8.8090(8) and 9.0510(12) Å in **2**, 8.6560(8) and 9.0430(8) Å in **3**, and 8.8850(15) and 11.260(2) Å in **6**, respectively. For **4**, distances of 8.7770(10) and 9.2681(11) Å correspond to the *a* and *c* directions, respectively. There are strong intermolecular C···C contacts within the layers ($\pi-\pi$ overlap), while these contacts do not occur between layers except for compound **1** (see Table 5).

Compounds **1** and **2** have a similar distribution of the anions and solvent molecules, which are located between the layers. A first interlayer space is filled with [BF$_4$]$^-$ ions; the adjacent interlayer space is filled with water molecules and [BF$_4$]$^-$ ions, and this sequence repeats to infinity. The most noticeable difference between **1** and **2** corresponds to the disposition of the water molecules and anions in the second layer. While the water molecules and [BF$_4$]$^-$ ions alternate homogeneously at constant separations in **2** (5.699(8) and 6.486(8) Å, respectively), this is not the case in **1** as, for instance, the [BF$_4$]$^-$ ions form "pairs" of ions separated by 4.456(6) Å, the distance between "pairs" being equal to 8.040(6) Å. Compound **3** displays a similar sequence as **1**, but now one interlayer space is filled with [SiF$_6$]$^{2-}$ ions and methanol molecules, while the other is filled with [BF$_4$]$^-$ ions. In compounds **4** and **6**, the anions and solvent molecules are distributed homogeneously in the interlayer space.

In general in the complex molecule, the solvent and the anions are involved in hydrogen bond interactions. In **1**, the OH group of one of the 4-terpyridone ligands of the complex, O(1), is hydrogen bonded to the oxygen atom of the water molecule, O(3), which also forms a hydrogen bond with the F atom belonging to the [BF$_4$]$^-$ anion: O(1)···O(3) = 2.658(11) Å and O(3)···F(1) = 2.650(18) Å. These interactions are discrete and involve two adjacent [Co(4-terpyridone)$_2$]$^{2+}$ cations, two water molecules, and two [BF$_4$]$^-$ anions. Compound **2** displays a different arrangement of the hydrogen bonds: the O(1) forms a hydrogen bond with O(3) (O(1)···O(3) = 2.635(9) Å), and this interacts with the F(6) and F(8) atoms of two anions (O(3)···F(6) = 2.750(13) Å and O(3)···F(8) = 2.9291(16) Å), defining infinite helicoidal chains. In **3**, the [BF$_4$]$^-$ and [SiF$_6$]$^{2-}$ anions form hydrogen bonds with the OH group of the ligands, the former with the O(2) and the latter with the O(1) (O(2)···F(2) = 2.706(4) Å and O(1)···F(5) = 2.565(3) Å). In addition, the [SiF$_6$]$^{2-}$ forms a hydrogen bond with the methanol molecule

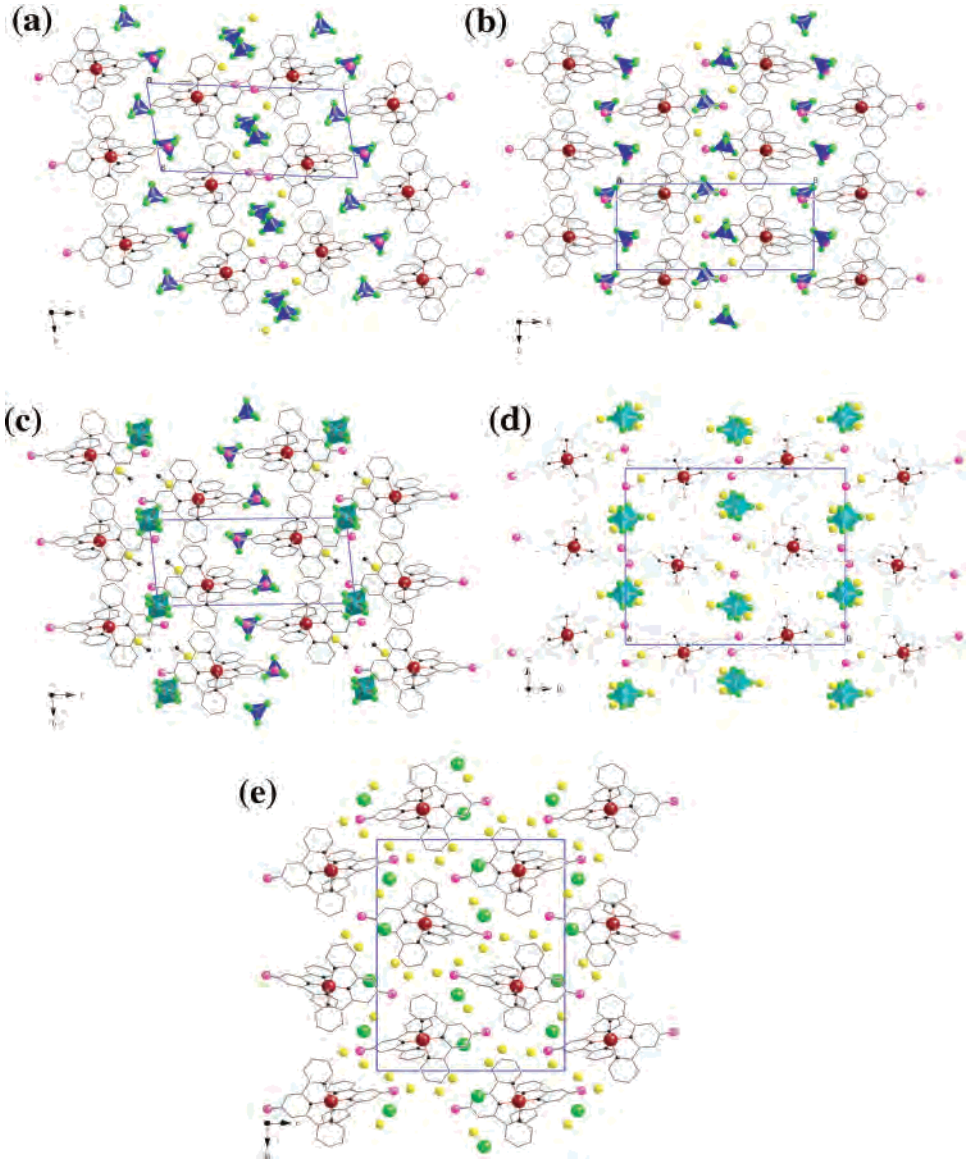

Figure 2. Crystal packing of complexes **1** (a), **2** (b), **3** (c), **4** (d), and **6** (e) along the *a* direction, illustrating the relative disposition of the complex cations, anions, solvent molecules, and the hydrogen bonds between them.

(O(3)···F(6) = 2.741(4) Å). Compound **4** displays one-dimensional arrays of hydrogen bonds spreading along the *c* axis. The OH groups of the 4-terpyridone ligands interact differently: the O(1) atom forms a hydrogen bond with the F(6) atom of the $[SiF_6]^-$ group, 2.500(7) Å, while the O(2) atom interacts with the water molecule, O(6), 2.575(8) Å. In addition, this O(6) atom forms two other hydrogen bonds: one with a methanol molecule (O(6)···O(3) = 2.666-(15) Å) and one with the F(5) atom of the $[SiF_6]^-$ group (2.696(9) Å). Infinite chains of complex molecules running along the *c* axis are also formed in **6**. The anion, I^-, is not involved in the hydrogen bonds: only the water molecules are involved (O(1)···O(7) = 2.562(10) Å, O(2)···O(5) = 2.734(8) Å, and O(5)···O(7) = 2.664(9) Å).

Formally, the crystal packing of **5** and **7** can be described as being composed of cationic complexes organized in parallel layers spreading on the *bc* plane (Figure 3). Each layer is made up of parallel chains of cations running along the *c* direction. The cationic complexes of two consecutive chains are rotated approximately 90° so that the lines connecting the two OH groups in one chain are almost perpendicular to those in the adjacent layer. As a result of this molecular orientation, the OH groups of consecutive chains define one-dimensional arrays of complex cations strongly hydrogen bonded (O(1)···O(2) = 2.455(5) (**5**) and 2.471(4) Å (**7**)) running parallel to the *b* axis. Within a plane, there are also strong C···C short contacts between the aromatic rings: in **5** these interactions spread on the whole layer (C(7)···C(24) = 3.482(6) Å, C(8)···C(9) = 3.409(9) Å, and C(8)····$C(8)^i$ = 3.318(9) Å (i = $-x$, $-y$, 2 − z)), while they are discrete in **7**, coupling two adjacent complexes (C(1)···C(2) = 3.480(7) Å, C(1)···C(3) = 3.571(7) Å, and C(2)···$C(2)^i$ = 3.434(7) Å (i = $-x$, $-y$, $-z$)). There is also an additional C···C interaction, 3.558(5) Å, between two consecutive layers involving atoms C(18) and C(30). The anions are located between the layers mentioned above, and only short C···C contacts have been observed between $[Co(NCS)_4]^{2-}$ and the aromatic rings (see Table 5).

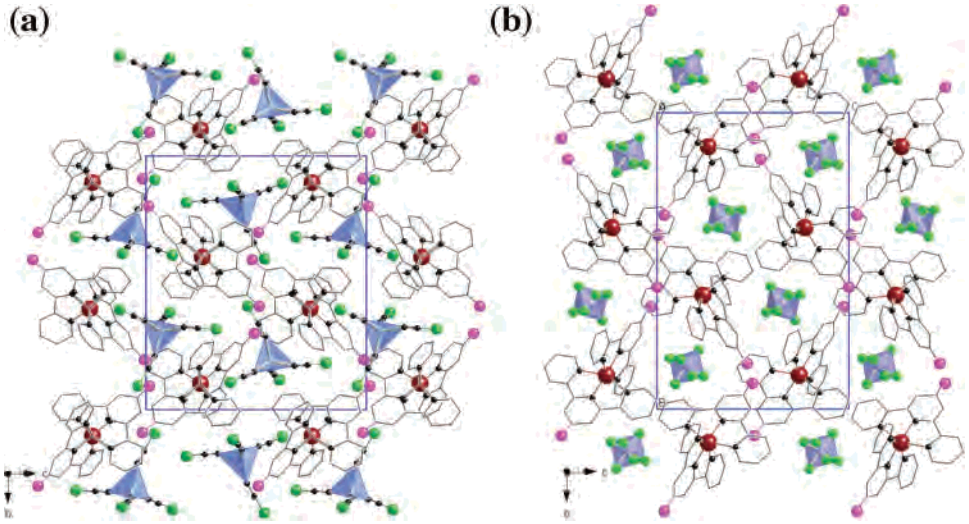

Figure 3. View of the molecular packing of **5** (a) and **7** (b) on the *bc* plane.

Magnetic Behavior of 1−8. The magnetic data expressed in the form of $\chi_M T$ versus T, χ_M being the molar magnetic susceptibilty and T the temperature, is shown in Figure 4 for polymorphs **1** and **2**. The magnetic behavior of **2** is very similar to that observed for the perchlorate derivative[23] showing a strong temperature dependence in the 5−340 K temperature range. At 340 K, $\chi_M T$ is equal to 2.48 cm^3 K mol^{-1}, a value which is consistent with that expected for a Co(II) ion in the HS state ($S = 3/2$) with orbital contribution ($g = 2.3$). The $\chi_M T$ values decreases continuously, upon cooling, attaining a value of 0.46 cm^3 K mol^{-1} at 100 K. Below 100 K, $\chi_M T$ remains practically constant down to 4 K. This $\chi_M T$ value corresponds to the LS state ($S = 1/2$, $g = 2.21$). This behavior is characteristic of a poorly cooperative $S = 1/2 \leftrightarrow S = 3/2$ spin transition. Indeed, the $\chi_M T$ versus T curves measured in the cooling−warming modes superimpose perfectly, indicating that no hysteresis occurs in this spin conversion. The characteristic temperature of the SCO for which 50% of HS and LS molecules coexist, $T_{1/2}$, is 152 K.

To estimate the relevant thermodynamic parameters associated with the spin transition, we have simulated the experimental data (see Supporting Information) using the regular solution model (eq 1)[25]

$$\ln\left[\frac{(1 - n_{HS})}{n_{HS}}\right] = \left[\frac{\Delta H + \Gamma(1 - 2n_{HS})}{RT}\right] - \frac{\Delta S}{R} \qquad (1)$$

where ΔH, ΔS, and Γ are the enthalpy and the entropy variations, and the parameter accounting for cooperativity associated with the spin conversion, respectively. The HS molar fraction, n_{HS}, can be expressed as a function of the magnetic susceptibility through (eq 2)

$$n_{HS} = [(\chi_M T)_m - (\chi_M T)_{LS}]/[(\chi_M T)_{HS} - (\chi_M T)_{LS}] \qquad (2)$$

where $(\chi_M T)_m$ is the value of $\chi_M T$ at any temperature and $(\chi_M T)_{LS}$ and $(\chi_M T)_{HS}$ correspond to the pure LS and HS states, respectively. In the present case, we have considered that the spin conversion is complete at low temperature, hence, $(\chi_M T)_{LS} = 0.458$ cm^3 K mol^{-1}, and that $(\chi_M T)_{HS}$ is an adjustable parameter. Least-squares fitting leads to $\Delta H = 3.04$ kJ mol^{-1}, $\Delta S = 20$ J K^{-1} mol^{-1}, $\Gamma = 0.95$ kJ mol^{-1}, and $(\chi_M T)_{HS} = 3.0$ cm^3 K mol^{-1}, which suggests the occurrence of 16.6% LS molecules at room temperature. These parameters are quite reasonable compared with those previously reported for cobalt(II) spin-crossover complexes.[7−12,23] The value of ΔS is much greater than the electronic spin change expected for a cobalt(II) ion: $\Delta S_{spin} = R \ln [(2S + 1)_{HS}/(2S + 1)_{LS}] = 5.8$ J K^{-1} mol^{-1}. The remainder entropy variation, 14.2 J K^{-1} mol^{-1}, is mainly the result of intramolecular vibrational changes. It should be noted that the value of ΔH (3.04 kJ mol^{-1}, 252 cm^{-1}) corresponds in a first approximation to the upper limit for the difference in energy, ΔE_{HL}, between HS and LS states. This gap appears to be small as compared with the ranges obtained for various [Co(terpy)$_2$]$^{2+}$ complexes, $\Delta E_{HL} = 1110-1700$ cm^{-1} and $\Delta E_{HL} = 300-500$ cm^{-1},[7] but somewhat larger than for the [Co(H$_2$-fsa$_2$en)L$_2$] complexes, $\Delta E_{HL} = 158-200$ cm^{-1}.[10,11] Such a doublet−quartet separation may be accounted for the lower $T_{1/2}$ and the expected stronger and weaker ligand field associated with 4-terpyridone with respect to (H$_2$-fsa$_2$en)-L and terpy, respectively.

For **1**, $\chi_M T$ is almost constant in the 5−175 K temperature range with a value of around 0.404 cm^3 K mol^{-1}. This value is consistent with a $S = 1/2$ ground spin state that follows a Curie−Weiss law with $g = 2.08$ and $\theta = -0.032$ K (see Supporting Information). When the sample is warmed, $\chi_M T$ smoothly increases, attaining a value of 1.53 cm^3 K mol^{-1} at 300 K. This behavior indicates the occurrence of an incomplete and poorly cooperative $S = 1/2 \leftrightarrow S = 3/2$ conversion at 300 K. Cooling−warming cycles in the temperature range of 300−5 K gives exactly the same behavior. However, $\chi_M T$ displays an abrupt increase, reaching a value of 2.47 cm^3 K mol^{-1}, in the temperature range of 325−338 K. Then $\chi_M T$ remains practically constant up to 350 K indicating that the $S = 1/2 \leftrightarrow S = 3/2$ conversion is rather complete. Subsequently, the $\chi_M T$ versus T curve was

(25) Slichter, C. P.; Drickamer, H. G. *J. Chem. Phys.* **1972**, *56*, 2142.

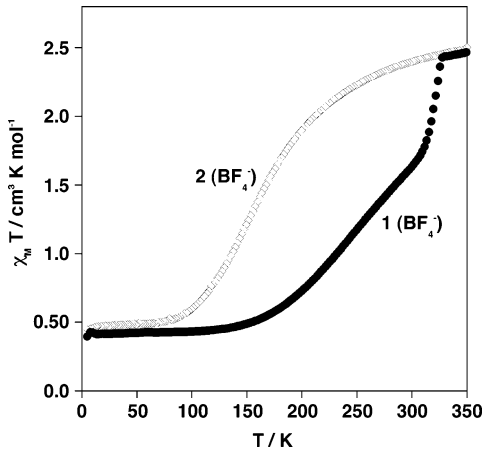

Figure 4. Magnetic properties of complexes **1** and **2** in the form of $\chi_M T$ vs T recorded in the cooling and warming modes at the rate of 1 K/min.

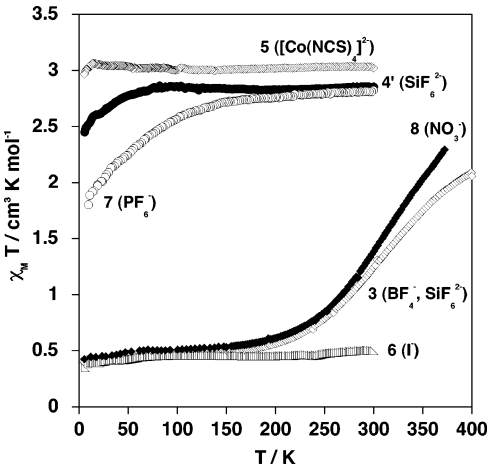

Figure 5. Magnetic properties of complexes **3**−**8** in the form of $\chi_M T$ vs T recorded in the cooling and warming modes at the rate of 1 K/min.

recorded in the cooling mode. Surprisingly, in this measuring mode, the magnetic behavior does not follow that of the warming mode but instead follows that described for **2**. After many cooling−warming cycles, **1** does not restore the magnetic curve formerly described. This anomalous behavior suggests the occurrence of an irreversible crystallographic phase transition which has been monitored by X-ray single-crystal diffraction. Indeed, a single crystal of **1** warmed to 340 K and subsequently cooled to 300 K displayed cell parameters identical to those observed for **2**.

Except for the singularity observed above 325 K, the temperature dependence of $\chi_M T$ for compounds **3** and **8** are similar to that of **1**. $\chi_M T$ is ca. 0.44 cm^3 K mol^{-1} and is practically constant in the 5−150 K temperature region, a value which is consistent with the LS ground state ($S = 1/2$ and $g = 2.27$). When the samples are warmed above 150 K, $\chi_M T$ progressively increases, attaining a value of 2.10 cm^3 K mol^{-1} (**3**) at 400 K and 2.30 cm^3 K mol^{-1} (**8**) at 370 K. This magnetic behavior shows the occurrence of an incomplete $S = 1/2 \leftrightarrow S = 3/2$ spin conversion at high temperatures.

For compounds **4′** ($n = 1CH_3OH{\cdot}1H_2O$ see discussion), **5,** and **7**, $\chi_M T$ is equal to 2.86, 3.03, and 2.81 cm^3 K mol^{-1}, respectively, in the 300−100 K temperature range. Then, $\chi_M T$ decreases upon cooling to 2.44 (**4′**) and 1.88 cm^3 K mol^{-1} (**7**) at 2 K, while it is practically constant for **5**. The magnetic behavior of **4′** and **7** is typical for HS Co(II) pseudo-octahedral complexes with noticeable orbital contributions, whereas **6** shows the typical behavior of a Co(II) in the LS state.

Like **4′** and **7**, the magnetic properties of **5** could be attributed to a pseudo-octahedral Co(II) HS complex, but in fact, they correspond to the sum of two components, one is LS ($S = 1/2$) and another HS ($S = 3/2$), belonging to the $[Co(4\text{-terpyridone})_2]^{2+}$ octahedral and to the $[Co(NCS)_4]^{2-}$ tetrahedral species, respectively.

Discussion

Here we have reported the synthesis and characterization of a series of new mononuclear Co(II) SCO complexes based on the 4-terpyridone ligand, $[Co(4\text{-terpyridone})_2]X_p{\cdot}nS$ where $X = BF_4^-$, SiF_6^-, PF_6^-, NO_3^-, $[Co(NCS)_4]^{2-}$, and I^- and $S = H_2O$ and MeOH. The spin state of the $[Co(4\text{-terpyridone})_2]^{2+/1+}$ cation appears to be dependent on either (or both) the solvent molecules or the accompanying anion.

The influence of the noncoordinating anion on the SCO process was first reported for salts of the complex cation $[Co(terpy)_2]^{2+}$[7,8] and later for the iron(II) systems $[Fe(paptH)_2]^{2+}$ (paptH = 2-(pyridin-2-yl-amino)-4-(pyridin-2-yl)thiazole)[26] and $[Fe(pic)_3]^{2+}$ [27−29], to list a few. Now, a plethora of iron(II), iron(III), and cobalt(II) SCO salts illustrate the influence of noncoordinating anions on the SCO process.[1−5] These influences may provoke drastic changes in the nature of the spin transition, for example from abrupt to continuous, or the displacement of the transition temperature and even the spin-crossover behavior can be suppressed. Hydrogen bonding has also been found to play a significant role in changes in the SCO behavior accompanying hydration/dehydration processes. It has been suggested that hydration will generally result in a stabilization of the LS state, through hydrogen bonding of the water with the ligand. This does seem to be the case for most hydrates, but in a cationic SCO system where the ligand is hydrogen bonded to the associated anion only and this in turn is bonded to the water, the effect can be the reverse (i.e., loss of water can also result in stabilization of the LS state).[1]

The 4(1H)-pyridone ring of the 4-terpyridone ligand switches to the 4-hydroxy form upon coordination to the metal ion. This OH group is the obvious difference between the complexes derived from 4-terpyridone and terpy. Despite this, both types of derivatives are similar and no further noticeable structural differences deserve to be noted. However, the presence of the OH group determines the differences observed in the supramolecular organization of the crystal packing. The crystal packing of the $[Co(4\text{-terpy})_2](X)_2{\cdot}nS$ series is very similar to that described for **1**−**4** and **6** when

(26) Sylva, R. N.; Goodwin, H. A. *Aust. J. Chem.* **1967**, *20*, 479.
(27) Renovitch, G. A.; Baker, W. A. *J. Am. Chem. Soc.* **1967**, *89*, 6377.
(28) Wiehl, L.; Kiel, G.; Köhler, C. P.; Spiering, H.; Gütlich, P. *Inorg. Chem.* **1986**, *25*, 1565.
(29) Hostettler, M.; Törnroos, K. W.; Chernyshov, B. V.; Bürgi, H. B. *Angew. Chem., Int. Ed. Engl.* **2004**, *43*, 4589.

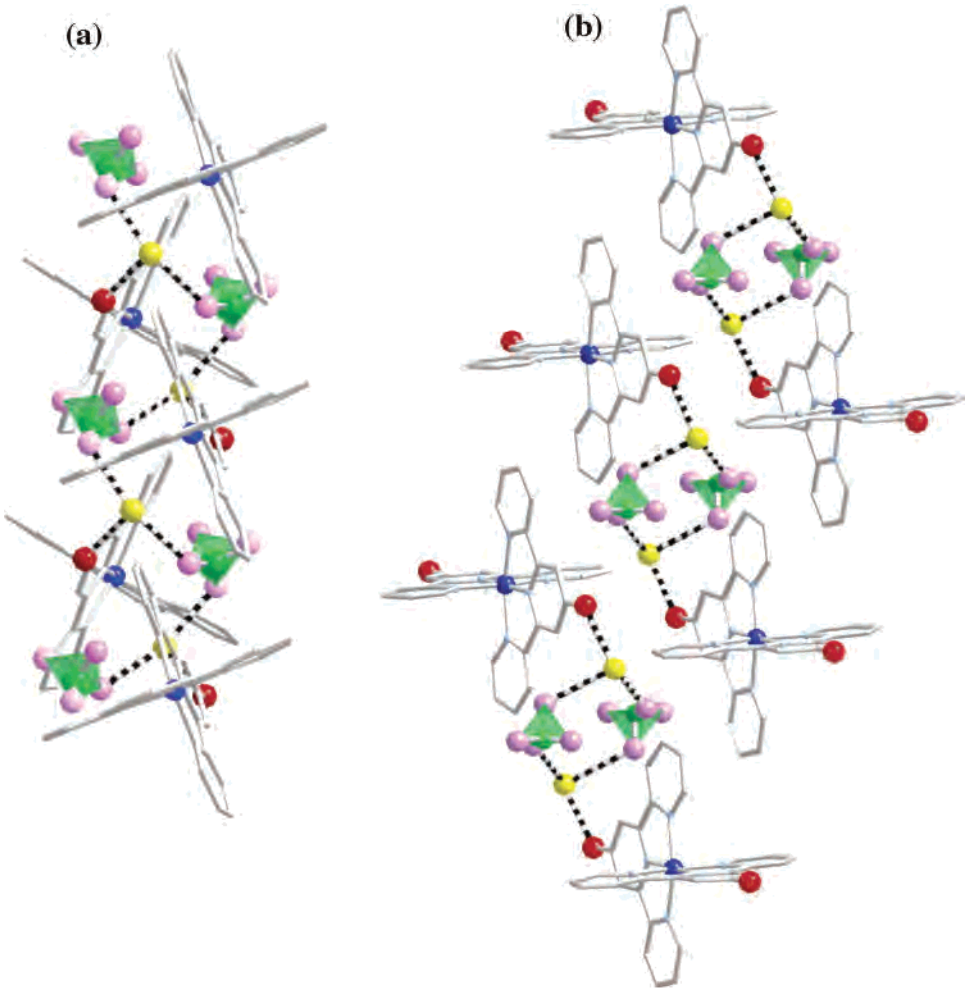

Figure 6. Different arrangements of the hydrogen bonds in **2** (a) and **1** (b).

the crystal packing is projected in the *bc* plane; namely, it consists of layers of cations spreading in the *ab* plane in which short C···C contacts determine the cohesive force between the cations. These planes stack along the *c* direction. However, the projection of the crystal packing in the *ab* plane is rather different for both series of complexes. In this respect, Figgis and co-workers have demonstrated that although the symmetries and cells of the [Co(terpy)$_2$](X)$_2$·*n*S system can change considerably, the geometry within the cation *ab* planes and the separation between the adjacent planes changes very little as a result of the lattice constraints imposed by the differing anions and number of waters of crystallization.[8] This is not true for **1**−**7**, as the 4-hydroxyl groups, not existing in the terpy derivatives, are strongly involved in hydrogen-bond interactions with the solvent molecules, the anions, or with other 4-hydroxyl groups of adjacent cations (i.e., **5** and **7**), and these interactions are different for **1**−**7**. In particular, it is worth mentioning the polymorphs **1** and **2**, as they represent a rare and interesting example of how intermolecular hydrogen bond interactions may play a fundamental role in determining the nature of the SCO behavior. Both polymorphs have different arrangements of the hydrogen bonds, these interactions are discrete in **1** and involve two OH groups belonging to two adjacent [Co(4-terpyridone)$_2$]$^{2+}$ cations, two water molecules, and two BF_4^- anions (Figure 6b). Strong hydrogen bonds give rise to the formation of infinite helicoidal chains made up of [Co(4-terpyridone)$_2$]$^{2+}$, BF_4^-, and H_2O molecules in **2** (Figure 6a), which should favor a more effective transmission of the structural changes associated to the spin change through the whole crystal. In fact, the SCO appears to be more cooperative and takes place at lower temperatures in **2** than in **1**. A further remarkable feature is the irreversible phase transition occurring in polymorph **1** when the temperature is higher than 325 K, leading to a more stable form whose magnetic behavior is that of polymorph **2**. The corresponding crystallographic transition from the triclinic $P\bar{1}$ (**1**) to the monoclinic $P2_1$ space group (**2**) has been confirmed from X-ray single-crystal diffraction. To the best of our knowledge, this is the first Co(II) SCO complex in which such a crystallographic phase transition has been characterized.

Compound **4** is an interesting example of the influence of the solvent molecules on the spin state of the cobal(II) ion. During the X-ray single-crystal experiments, we became aware of its possible efflorescent nature. This was the reason the single crystals were preserved in sealed tubes. The lattice contains three molecules of CH_3OH and one molecule of H_2O per formula, and the average Co−N bond distance is $R = 2.028$ Å. It is well-known that R depends linearly on the degree of spin conversion (i.e., on the high-spin molar

fraction). For the LS and HS complexes in this series, R_{LS} and R_{HS} are equal to 1.919 (i.e., **5** and **6**) and 2.118 Å (i.e., **7**), respectively. It is important to emphasize that the difference, $\Delta R_{LH} = 0.199$ Å, cannot be used as a reference of the change expected for a SCO cobalt(II) complex, which is usually found to be around 0.1 Å. For the title SCO compounds, the *R* values are equal to 1.982, 2.064, and 2.035 Å; these values are consistent with the HS-to-LS conversion degree of **1**, **2**, and **3** at 293 K, respectively. Hence, the *R* value of **4** is close to that of **3**; however, the magnetic behavior of the former could not be recorded because of its efflorescent nature leading to **4′**, whose TGA analysis is consistent with the loss of one molecule of methanol and one of water (see Supporting Information). In fact the magnetic behavior of **4′** corresponds quite well to that of a HS complex (i.e., **7**). In other words, the partial loss of solvent switches the nature of **4** from SCO to HS (**4′**).

Finally, another significant singularity corresponds to the LS structure of compound **3**. This compound has $\chi_M T$ values of 1.73 cm^3 K mol^{-1} at 293 K and 0.44 cm^3 K mol^{-1} at 105 K. Considering a $\chi_M T$ value for the fully HS state to be equal to 2.8 cm^3 K mol^{-1} and that for the fully LS state to be equal to 0.44 cm^3 K mol^{-1}, approximately 62% of the cations are in the LS state at 293 K. Consequently, a subsequent 38% of HS-to-LS change takes place in the 293−105 K range. If a total change, ΔR, of 0.1 Å is expected for the total spin conversion, one should expect a ΔR values of ca. 0.03 Å. However, the *R* values at 293 and 105 K are 2.035 and 2.023 Å, respectively, and they give a ΔR value of 0.012 Å, which is noticeably smaller than the expected value. In this respect, it deserves to be noted that the central Co−N(5,2) and the distal Co−N(1,3) distances decrease when cooling in the 293−105 K region by ca. 0.013 and 0.041 in average. In contrast to the expected, the distal Co−N(4,6) bonds increase considerably (0.019 Å in average), mitigating the magnitude of the expected average bond-length contraction. The coordination octahedron is severely distorted (elongated); a situation that strongly contrasts with the LS structures displayed by **5** and **6**.

In summary, rationalization of the factors that govern the SCO process in cationic transition-metal complexes is rather difficult because they are not always consistent from one system to another and, in general, are not predictable.

Acknowledgment. Financial support is acknowledged from the Spanish Ministerio de Educacion y Ciencia (MEC) (CTQ 2004-03456/BQU). A.G. thanks the Universitat Politécnica de València for a predoctoral fellowship. A.B.G. thanks the Spanish MEC for a research contract (Programa Ramón y Cajal). We also acknowledge the European Project MAGMANET.

Supporting Information Available: Figure S1 showing the magnetic fitting of compounds **1** and **2**, Figure S2 showing the TGA of compound **4′**, and CIF data for compounds **1**−**7**. This material is available free of charge via the Internet at http://pubs.acs.org.

IC060090U